American Mineralogist, Volume 103, pages 1663–1673, 2018

Polyphase solid-inclusions formed by interactions between infiltrating fluids and precursor minerals enclosed in garnet of UHP rocks from the Dabie Shan, China

Penglei Liu[1,2,*], Junfeng Zhang[1], Hans-Joachim Massonne[2], and Zhenmin Jin[1]

[1]School of Earth Sciences, China University of Geosciences, 430074 Wuhan, China
[2]Institut für Mineralogie und Kristallchemie, Universität Stuttgart, Azenbergstrasse 18, D-70174 Stuttgart, Germany

Abstract

Three types of polyphase solid-inclusions (PSIs) with distinct mineral assemblages and microstructures were found in garnet of an ultrahigh-pressure (UHP) eclogite-vein system from the Dabie Shan, east-central China. Type-1 PSI contains variable volumes of quartz, K-feldspar, plagioclase ± other phases, whereas Type-2 PSI contains variable volumes of quartz, calcite ± other phases. Both types display shapes that are compatible with those of euhedral coesite inclusions. Type-3 PSI always contains a rutile core that is surrounded by plagioclase ± quartz and generally displays the morphology of the rutile core. Variable amounts of K-feldspar are embedded within the plagioclase of Type-3 PSIs. The three PSI types developed fluid-mediated microstructures that include wedge-like offshoot and protrusion textures and inclusion-garnet interfaces controlled by the crystallographic structure of garnet. PSIs in peak minerals of UHP rocks have been previously thought to represent primary supercritical fluid or melt inclusions. Here we propose that the studied PSIs were formed under high-pressure (HP) eclogite-facies conditions during exhumation and represent reaction products between an enclosed mineral, such as coesite and rutile, and external fluids infiltrating the host garnet along fractures that have been healed later on. Two immiscible aqueous fluids (i.e., a siliceous and a carbonaceous) were involved in the formation of these PSIs. The siliceous fluid was rich in various large ion lithophile elements like Cs, Rb, Ba, K, Pb, Li, and Sr, whereas the carbonaceous fluid was rich in Pb and Sr. The new PSI formation mechanism proposed in this study brings significant implications for tracing fluid evolution and post-entrapment modifications of mineral inclusions in HP and UHP metamorphic rocks.

Keywords: Dabie Shan, ultrahigh-pressure, coesite, polyphase solid-inclusion, fluid-rock interaction

Introduction

Ultrahigh-pressure (UHP) metamorphic rocks represent relicts of deeply subducted crust and provide a natural laboratory to study the nature and behavior of metamorphic fluids in deep-seated subduction zones. The knowledge of the interaction of these fluids is important for understanding the formation, preservation, rheology, and exhumation of UHP rocks and the possible mass transfer in subduction zones (e.g., Proyer 2003; Zhang et al. 2004; Massonne 2009; Labrousse et al. 2011; Zheng et al. 2011; Hermann et al. 2013; Frezzotti and Ferrando 2015). However, there are considerable difficulties to characterize these fluids at present. One big obstacle is that the metamorphic fluids in deep-seated subduction zones usually escape from their site of interaction and leave little traces of their activity in natural rocks. Whereas experimental and theoretical studies are crucial for deciphering the physical and chemical properties of fluids in deep-seated subduction zones (e.g., Zheng et al. 2011; Hermann et al. 2013; Hermann and Rubatto 2014), polyphase solid-inclusions (PSIs) in peak minerals such as garnet have been considered in the past two decades to be a good window for peering into UHP rocks affected by fluid interaction. Such inclusions commonly display an intergrowth of several daughter minerals, negative crystal shapes, and wedge-like offshoots, and they are interpreted to represent precursor supercritical fluid or melt inclusions (e.g., Hwang et al. 2001; Stöckhert et al. 2001, 2009; Ferrando et al. 2005; Korsakov and Hermann 2006; Malaspina et al. 2006; Frezzotti et al. 2007; Frezzotti and Ferrando 2015). Similar PSIs (known as nanogranitoids), crystallized from felsic melt, have been also reported in anatectic rocks of different crustal levels (e.g., Cesare et al. 2009, 2015; Ferrero et al. 2012, 2015; Bartoli et al. 2013). In all the reported cases, PSIs were normally considered primary, i.e., they were captured during growth of the host phases.

Among the reported PSIs in UHP rocks, one group, mainly composed of quartz, K-feldspar, and/or plagioclase, has attracted substantial attention. The petrogenesis of this group of PSI has been highly debated in the literature. Such PSIs have been interpreted as the reaction products between coesite inclusions and a K-bearing omphacite host (Yang et al. 1998), although their occurrence in garnet cannot be interpreted in the same way. Another opinion refers to the former presence of composite K-cymrite + coesite inclusions (Massonne 2001; Massonne and Nasdala 2003; Song et al. 2003; Zhang et al. 2009), but it cannot account for the occurrence of larger quantities of plagioclase and/or other minerals within such PSIs. In the light of recent studies, which suggest that these PSIs could represent entrapped melts (e.g., Zeng et al. 2009; Gao et al. 2012, 2013, 2017; Liu et al. 2013; Chen et al. 2014), we present here new perspectives on the formation of

* E-mail: liupengleiincug@aliyun.com

0003-004X/18/0010–1663$05.00/DOI: http://doi.org/10.2138/am-2018-6395

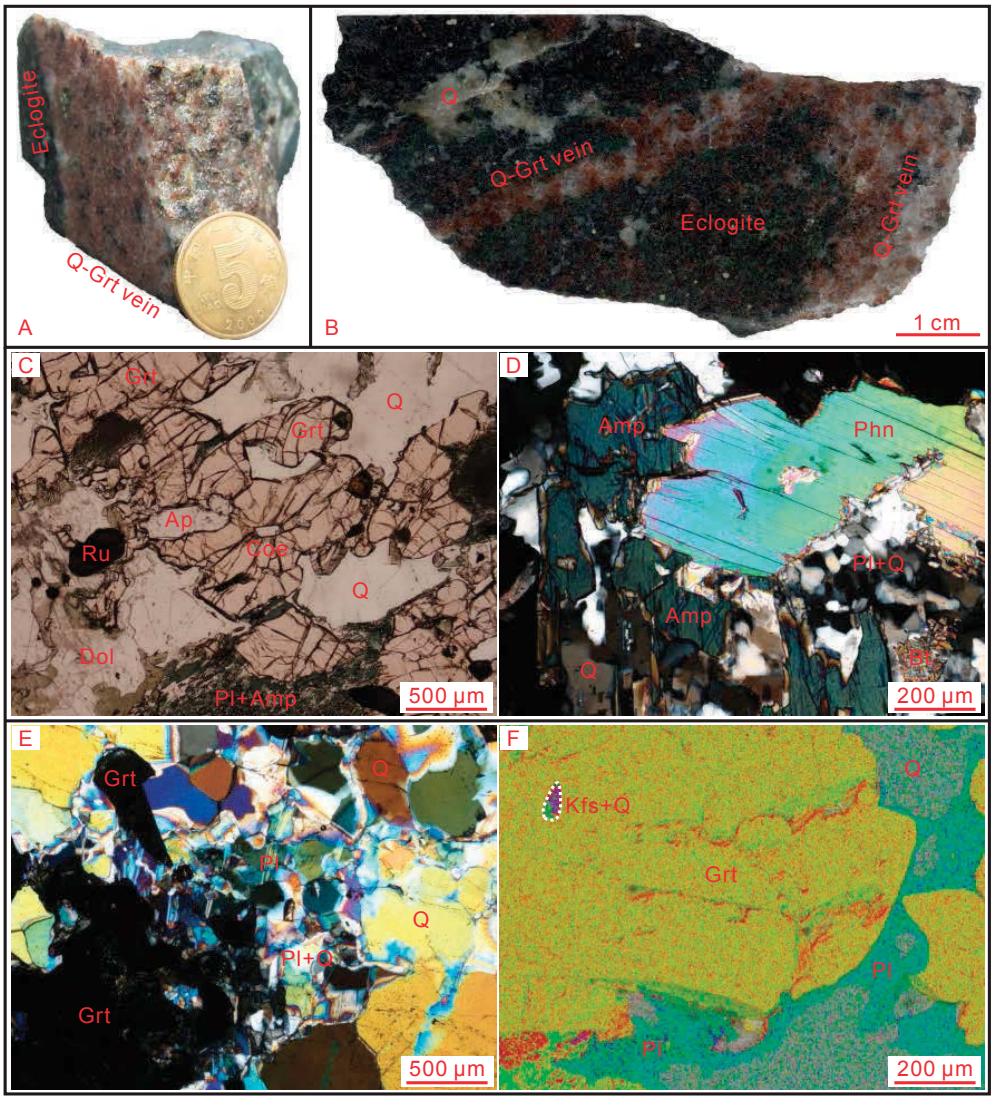

FIGURE 1. (**a**) Photograph and (**b**) scanned image of two sections cut from the eclogite-vein system (sample GJL12-4). The coin in **a** is 2 cm in diameter. (**c**–**e**) Photomicrographs and (**f**) mixed mapping image of eclogite (**c** and **d**) and quartz-garnet veins (**e** and **f**). Mineral abbreviations in this study: Ab = albite, Alm = almandine, Amp = amphibole, An = anorthite, And = andradite, Ap = apatite, Bt = biotite, Cal = calcite, Chl = chlorite, Cn = celsian, Coe = coesite, Dia = diamond, Dol = dolomite, Ep = epidote, Gra = graphite, Gro = grossular, Grt = garnet, Ilm = ilmenite, Jd = jadeite, Kfs = K-feldspar, Or = orthoclase, Phn-phengite, Pl = plagioclase, Prp = pyrope, Py = pyrite, Q = quartz, Ru = rutile, Sp = spessartine, Ttn = titanite, Zr = zircon. (Color online.)

quartz-feldspar-bearing PSIs in UHP rocks based on microstructural observations and a geochemical study on their counterparts in garnet of an eclogite-vein system from the Dabie UHP terrane, eastern China. Unlike primary PSIs, we demonstrate unequivocally that these PSIs represent reaction products between precursor minerals (coesite and rutile) in the inclusions and external fluids infiltrating the host garnet along fractures that have been healed later on. Instead of melts, two immiscible aqueous fluids (i.e., a siliceous and a carbonaceous) are proposed to have been involved in the formation of the investigated PSIs.

SAMPLE LOCATION AND ANALYTICAL METHODS

The studied sample GJL12-4, collected from the Ganjialing area (N 30°38.666′, E 116°19.619′) in the Dabie UHP terrane, east-central China, is a decimeter-sized loose boulder of eclogite hosting centimeter-sized quartz-garnet veins (Figs. 1a and 1b). This boulder coexists with impure marbles in the field but the contact relationship is unclear. Former studies of the impure marbles have led to the discovery of coesite inclusions in dolomite and the derivation of peak *P-T* conditions of 4.2 ± 0.3 GPa and 745 ± 65 °C (Liu et al. 2015). In addition, intergranular coesite has been found in a metasedimentary rock from the same outcrop (Liu et al. 2017a). Descriptions of the geological background and regional geology of this outcrop can be found in Liu et al. (2015, 2017b).

The petrography of sample GJL12-4 was examined on thin sections using an optical microscope and a FEI Quanta 450 FEG scanning electron microscope (SEM) at the State Key Laboratory of Geological Processes and Mineral Resources (GPMR), China University of Geosciences (CUG), Wuhan. The SEM is equipped with an Oxford INCA X-Max 50 energy-dispersive X-ray (EDX) spectrometer, which was used to identify tiny minerals and to map PSIs. The working conditions were 20 kV accelerating voltage, 5–6 μm spot size, and 12–15 mm working distance.

The major element chemistry of minerals was measured using a JEOL JXA-8100RL electron microprobe (EMP) with four wavelength-dispersive X-ray (WDX) spectrometers and an EDX spectrometer at the GPMR. An accelerating voltage of 15 kV and a beam current of 20 nA were applied. A beam diameter between 1 and 5 μm was selected depending on the character of the analyzed mineral and its size. The counting times were 10 s for Na, K, Mg, Ca, and Al; 20 s for Cr, Ti, Fe, and Si; 15 s for Mn; and 30 s for Ba at peak and background. The ZAF method was used for data correction. Natural and synthetic silicates and oxides were used as standards. X-ray maps of selected garnet grains containing PSIs were obtained in WDX mode using a CAMECA SX100 EMP at the Institut für Mineralogie und Kristallchemie, Universität Stuttgart. An accelerating voltage of 15 kV, a beam current of 50 nA, a step size of 2–3 μm, and a dwell time of 100 ms were applied.

The trace element chemistry of garnet and PSIs was analyzed in situ on thin sections by a laser ablation-inductively coupled-mass spectrometer (LA-ICP-MS) at the GPMR. Laser sampling was performed with a GeoLas 2005 system. The laser beam size, frequency, and energy were set to 44 (for garnet) or 60 μm (for PSIs), 6 Hz, and 70 mJ, respectively. An Agilent 7500a ICP-MS was used to determine ion-signal intensities. Helium (He) was used as the carrier gas and mixed with Argon (Ar) through a T-connector before entering the ICP. Nitrogen was imported into the central gas flow (Ar + He) of the Ar plasma to improve the detection limits and precision. For each analysis, the Agilent Chemstation was used to incorporate a background acquisition of 20–25 s and a subsequent 50 s acquisition for the sample. Offline selection and integration of background and analytical signals, time-drift correction, and quantitative calibration were performed by the software ICPMSDataCal (Liu et al. 2008). Element concentrations were calibrated against multiple reference materials BIR-1G, BCR-2G and BHVO-2G without using an internal standard (Liu et al. 2008).

Sample descriptions

Both the eclogite and the quartz-garnet veins display a fine- to medium-grained texture (Figs. 1c–1f). The eclogite partially preserved the peak mineral assemblage of garnet, phengite, coesite, dolomite, rutile, apatite (Figs. 1c and 1d), omphacite, and magnesite. Garnet (ca. 40 vol%), occurring as anhedral to subhedral grains (0.1–1.5 mm), contains inclusions of coesite (Fig. 1c), omphacite, rutile, apatite, and zircon. Omphacite in the matrix has been totally replaced by amphibole + plagioclase symplectites (Fig. 1c). Phengite is often partially replaced by plagioclase + quartz pools that embed biotite clusters (Fig. 1d). Xenoblasts and coronae (around garnet, phengite, and dolomite) of amphibole and epidote are additional retrograde products. Dolomite (ca. 5–10 vol%) constitutes an important rock-forming mineral (Fig. 1c), whereas magnesite only occurs as an accessory phase.

The quartz-garnet veins display a sharp contact to the host eclogite (Figs. 1a and 1b). At their boundaries, amphibole + plagioclase symplectites in the eclogite are texturally preserved, without evidence of interaction with the veins. The veins comprise mainly garnet (ca. 40–45 vol%), quartz (ca. 40–45 vol%), and plagioclase (ca. 5–7 vol%) (Fig. 1e). Minor and accessory mineral phases are amphibole, epidote, apatite, phengite, K-feldspar, chlorite, calcite, rutile, ilmenite, titanite, sulfide, and zircon. Garnet (0.1–1.8 mm) in the veins displays a similar texture to that in the eclogite. It is partially replaced by amphibole or epidote in places and contains inclusions of quartz, rutile, apatite, and zircon. Plagioclase occurs as thin films or wide bands along the grain boundaries of garnet, quartz (Fig. 1f), apatite, and rutile, which grade into irregular pools in places (Fig. 1e). Relict coesite and polycrystalline quartz aggregates typically replacing coesite were not found in the vein garnet, but the prismatic and platy morphologies of some quartz inclusions (Figs. 2a and 2b) still suggest that they inherit their shapes from former coesite. The quartz inclusions display specific microstructures like wedge-like offshoot and protrusion textures and inclusion-garnet interfaces controlled by the crystallographic structure of garnet (Fig. 2). In addition, small garnet blebs can be rarely found in quartz inclusions (Fig. 2d).

PSIs in garnet

PSIs are common in the vein garnet. A single garnet grain generally contains one to several PSIs that are distributed within this host mineral in a random way. The PSIs can be subdivided into three major types (1, 2, and 3) on the basis of their mineral assemblages and microstructures (Table 1). Type-1 PSIs comprise mainly variable volumes of quartz and feldspar (Figs. 3a–3k). Amphibole, epidote, titanite, ilmenite, calcite, chlorite, and pyrite also occur within Type-1 PSIs, but their occurrence and contents vary considerably in these inclusions. Three subtypes were defined for Type-1 PSIs (Table 1), which are those containing quartz + K-feldspar ± other accessory phases (Type-1A: Figs. 3a–3d), quartz + plagioclase ± other accessory phases (Type-1B: Figs. 3e–3g) and two feldspars ± other accessory phases (Type-1C: Figs. 3h–3k). Type-2 PSIs (Fig. 3l) contain variable volumes of quartz and calcite. In some of them chlorite, epidote, and/or titanite form well-defined patches. Type-3 PSIs always contain a rutile core that is surrounded by plagioclase ± quartz (Figs. 3m–3p). Variable amounts of K-feldspar are embedded within the plagioclase of Type-3 PSIs. The rutile core is usually partially replaced by ilmenite ± titanite (Figs. 3m–3o). All PSIs contain oval microcavities (Figs. 3c, 3g, 3i, 3l–3p) that could represent exposed fluid inclusions. Type-1 and Type-2 display regular or irregular shapes and sizes from 5 × 20 to 200 × 300 μm. The regular ones are generally prismatic or platy (Figs. 3a, 3c–3e, 3h, 3j). Both regular and irregular types developed wedge-like offshoot and protrusion textures (Figs. 3a–3d, 3k, and 3l) with serrated and straight garnet-inclusion interfaces (Figs. 3b, 3c, 3g, 3i, and 3l). Type-3 PSIs vary in size with diameters from tens of micrometers to more than 200 μm. Their general morphology is always similar to that of the rutile core (Figs. 3m–3p). Type-3 PSIs developed a protrusion texture as well (Fig. 3o). Their interfaces with the host garnet are controlled by the crystallographic structure of garnet, as indicated by the angles between some interfaces (Figs. 3m–3p). Although this feature is rare, it can be still traced for some Type-1 and Type-2 PSIs (Figs. 3f, 3i, and 3l). It should be noted that BSE-brighter vein-like domains occur around the PSIs in garnet (Figs. 3e, 3f, 3k, and 3l). These domains are cut by extant fractures that are locally sealed by chlorite (Fig. 3q).

Garnet in the eclogite contains rare Type-1 and Type-2 PSIs similar to those in the vein garnet (Figs. 3q–3s). Type-3 PSIs are

Table 1. Summary of mineral assemblages and microstructures of PSIs in the eclogite-vein system

PSI types	Mineral assemblages	Notes on mineral assemblages	Key microstructures
Type-1A	quartz + K-feldspar ± accessory minerals	Accessory amphibole, epidote, titanite, ilmenite, calcite, chlorite, and pyrite occur in Type-1 PSIs, but their occurrence and contents vary considerably.	Type-1 and Type-2 PSIs have similar microstructures: prismatic, platy, and irregular shapes; with wedge-like offshoot and protrusion textures; serrated and straight garnet-inclusion interfaces; surrounded by healed fractures.
Type-1B	quartz + plagioclase ± accessory minerals		
Type-1C	plagioclase + K-feldspar ± accessory minerals		
Type-2	quartz + calcite	Chlorite, epidote, and/or titanite may form well-defined patches in some Type-2 PSIs.	
Type-3	rutile core + surrounding plagioclase ± K-feldspar	Rutile core is usually partially replaced by ilmenite ± titanite. Quartz was only found in one Type-3 PSI.	With a general morphology of the rutile core and a protrusion texture; inclusion-garnet interfaces controlled by the crystallographic structure of garnet; surrounded by healed fractures.

common in the eclogite but hardly contain K-feldspar (Figs. 3t). Given that PSIs in the veins are much more abundant and representative, we will focus on the PSIs in the veins hereafter unless specifically stated.

EDX mapping was performed on some PSIs in the eclogite-vein system, which revealed more details on the mineral assemblages in the PSIs (Fig. 4). For instance, some mineral phases (e.g., plagioclase and quartz) in single PSIs have a similar color in backscattered electron (BSE) images but they can be easily distinguished by EDX mapping (Fig. 4).

Compositions of garnet and PSIs

WDX mapping reveals that the rim of garnet in the eclogite-vein system experienced fluid-mediated alteration because, among others, this garnet domain (zone B) displays a completely different composition compared to the unaltered garnet (zone A), where the PSIs are generally included (Fig. 5). Garnet alteration texturally related to the occurrence of the PSIs was not observed (Fig. 5). Regardless of the altered domain, garnet in the eclogite and in the veins is nearly compositionally homogeneous (Fig. 5). This mineral in the eclogite contains 44–50 mol% almandine, 32–39 mol% grossular, 14–18 mol% pyrope, and 1–2 mol% spessartine and shows a very similar composition to that in the veins: 43–50 mol% almandine, 32–41 mol% grossular, 12–17 mol% pyrope, and 1–2 mol% spessartine (Supplemental[1] Table S1). Also, the trace element contents in both garnets are nearly identical. When normalized against chondrite and primitive mantle, the rare-earth element (REE) patterns and spider diagrams of garnet are characterized by enrichment of the middle and heavy REEs (MREEs and HREEs) and Y and by the depletion of light REEs (LREEs) and the large-ion lithophile elements (LILEs: Cs, Rb, Ba, K, Pb, Li, and Sr; Supplemental[1] Table S2; Figs. 6a and 7a). Representative major-element chemistry of minerals constituting the PSIs is listed in Supplemental[1] Table S1. Both feldspars display a wide compositional range. The composition of plagioclase is $Ab_{73–100}An_{0–27}$. The K-feldspar can contain high BaO (0.85–14.5 wt%) but little Na_2O (0.19–1.22 wt%) and CaO (≤0.21 wt%) contents. According to the nomenclature of Leake et al. (1997), the amphibole can be classified as pargasite and tschermakite. This mineral contains 2.17–2.64 Al per formula unit (pfu) with $Mg/(Mg+Fe^{2+})$ ratios between 0.51 and 0.61. Only one spot analysis was obtained for epidote that contains 30 mol% pistacite. Chlorite shows an Mg/(Mg+Fe) ratio of 0.38. Titanite hosts 0.08–0.14 Al pfu. Calcite is nearly pure $CaCO_3$.

Only Type-1 and Type-2 PSIs were analyzed for their trace element chemistry. The used laser-beam size of 60 μm could cover the bulk inclusion in most selected cases. For several large PSIs, only a representative portion that contains all the inclusion phases was sampled. As shown later, this will not influence our explanations or change our conclusions. Moreover, variable volumes of garnet ≤50 vol% were sampled together with the PSIs. In total, 13 Type-1 PSIs (+ garnet) were analyzed (Supplemental[1] Table S3). Compared with the host garnet, the mixtures commonly exhibit a prominent increase of the contents of LILEs (Fig. 7a). Because these elements are negligible in garnet, they could be assigned to the PSIs. The mixtures also exhibit various increases of the contents of LREE and high field strength elements (HFSEs: Th, U, Nb, Ta, Ti; Supplemental[1] Table S3; Figs. 6a and 7a), which

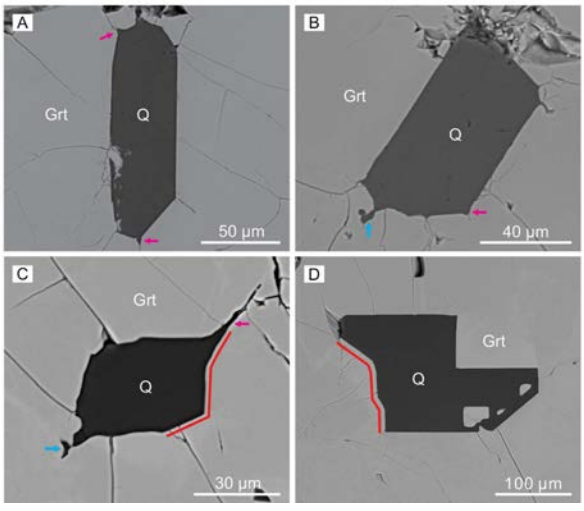

Figure 2. BSE images of monophase quartz inclusions within garnet of quartz-garnet veins. Wedge-like offshoot (pink arrows) and protrusion (blue arrows) textures and inclusion-garnet interfaces controlled by the crystallographic structure of garnet (red lines) are indicated. Note that some quartz inclusions display a prismatic (**a**) or platy (**b**) shape. (Color online.)

principally depend on the occurrence of some specific minerals within the PSIs. For example, the occurrence of epidote and titanite could cause the increase of the contents of LREE-Th-U and Nb-Ta-Ti, respectively (Supplemental[1] Table S3; Fig. 7a). In one case, the analyzed mixture displayed a remarkable increase of the contents of MREE-HREE-Y (Supplemental[1] Table S3; Figs. 6a and 7a) because the PSI contained Y-rich epidote proven by EDX analysis (Fig. 3c). In another case, high Zr and Hf contents were detected that could be related to micro-zircon beneath the thin section surface (Supplemental[1] Table S3; Fig. 7a).

To obtain the bulk compositions of pure Type-1 PSIs, chemical contributions of garnet to the mixtures were subtracted based on the mean composition of the unaltered garnet domains in the veins and estimated garnet volumes incorporated into single analyses (Supplemental[1] Tables S3 and S4). Nevertheless, such estimations are semi-quantitative and involve large uncertainties. The distribution patterns of the calculated trace element compositions are always similar to those of the mixtures (Figs. 6 and 7). They exhibit a nearly flat MREE-HREE distribution with LREE depletion, LILE enrichment and $U_N > Th_N$ (Figs. 6b and 7b). Negative Nb-Ta-Ti and Zr-Hf anomalies were usually observed unless titanite and/or zircon were ablated (Fig. 7b).

Two large Type-2 PSIs were partially analyzed without garnet (Supplemental[1] Table S3). As calcite and quartz distribute evenly within these two PSIs, the analytical results are supposed to be representative for the bulk inclusions. Compared to Type-1 PSIs, these two Type-2 PSIs contain much lower contents of trace elements except Pb and Sr (Supplemental[1] Table S4; Figs. 6b and 7b). Their REE patterns are similar to those of Type-1 PSIs (Fig. 6b). In the spider diagrams, they display positive Pb and Sr anomalies with the contents of most other LILEs and HFSEs below the primitive mantle values and/or the detection limits (Fig. 7b).

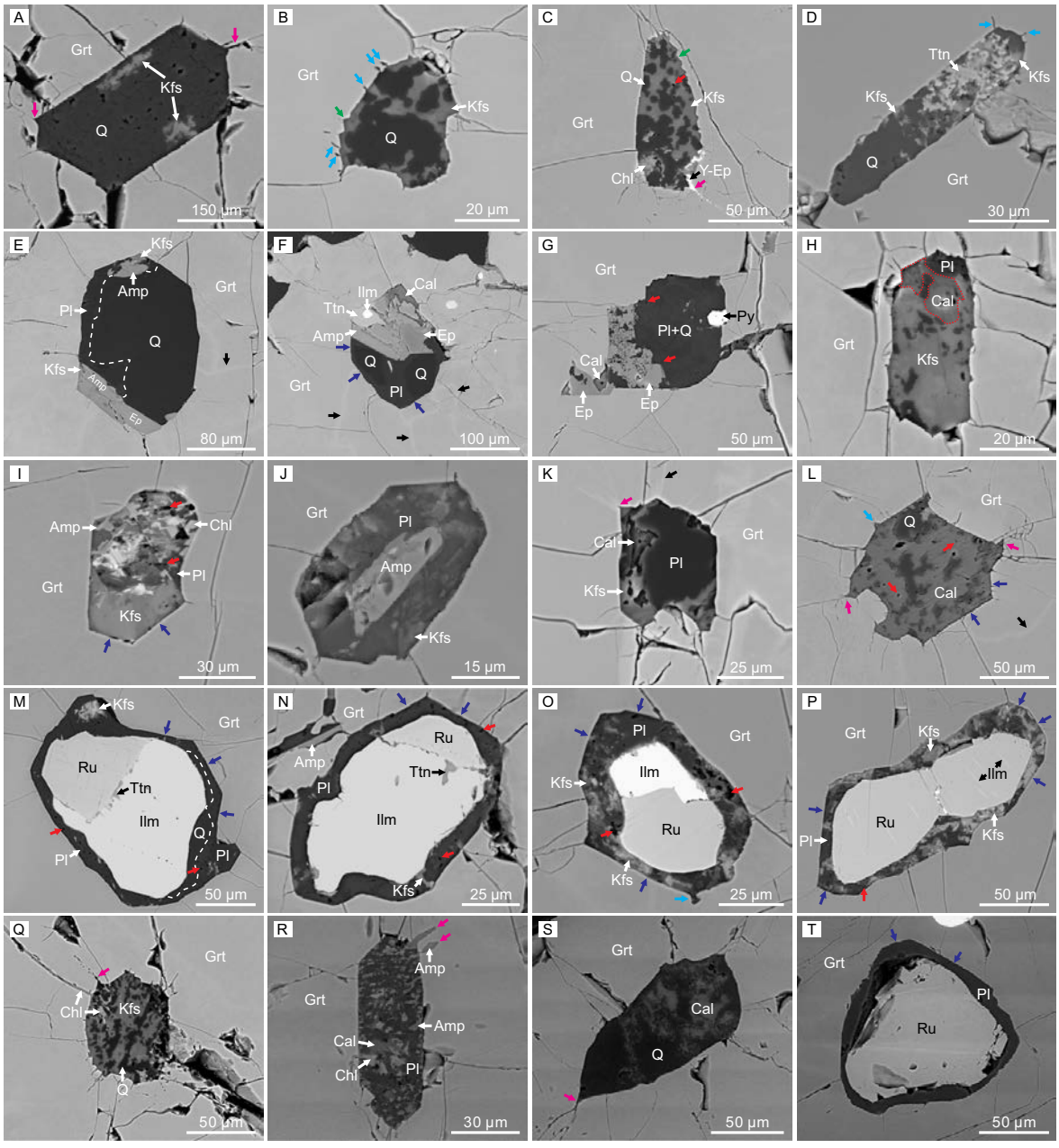

FIGURE 3. BSE images of PSIs within garnet of quartz-garnet veins (**a**–**p**) and eclogite (**q**–**t**). Three PSI types can be recognized: Type-1 (**a**–**k**, **q**, **r**), Type-2 (**l**, **s**), and Type-3 (**m**–**p** and **t**). See text in details. Healed fractures (black arrows), wedge-like offshoot (pink arrows) and protrusion (light blue arrows) textures, serrate inclusion-garnet interfaces (green arrows), possible crystal faces of garnet (dark blue arrows), and exposed fluid inclusions (red arrows) are indicated. (Color online.)

GENERAL ASPECTS RELATED TO THE FORMATION OF THE ECLOGITE-VEIN SYSTEM

Garnet in the eclogite contains coesite inclusions (Fig. 1c) suggests that the eclogite experienced UHP metamorphism. Applying conventional geothermobarometry, Liu et al. (2015) constructed a *P-T* path for the impure marbles that coexist with the eclogite-vein system. This *P-T* path is characterized by peak *P-T* conditions of 4.2 ± 0.3 GPa and 745 ± 65 °C that were followed by a nearly isothermal exhumation before late amphibolite-facies overprint. Preliminary work on the eclogite *P-T* evolution points to a similar *P-T* path but with somewhat lower peak *P-T* conditions ($P \geq 3.7$ GPa; T around 700 °C; Fig. 8).

Petrographic features described above suggest that the quartz-garnet veins within the eclogite formed by fluid infiltration during exhumation. The corresponding fluid-rock interactions should have proceeded along fractures that had developed in the eclogite (Fig. 1b). Three different fluid-mediated processes could have been

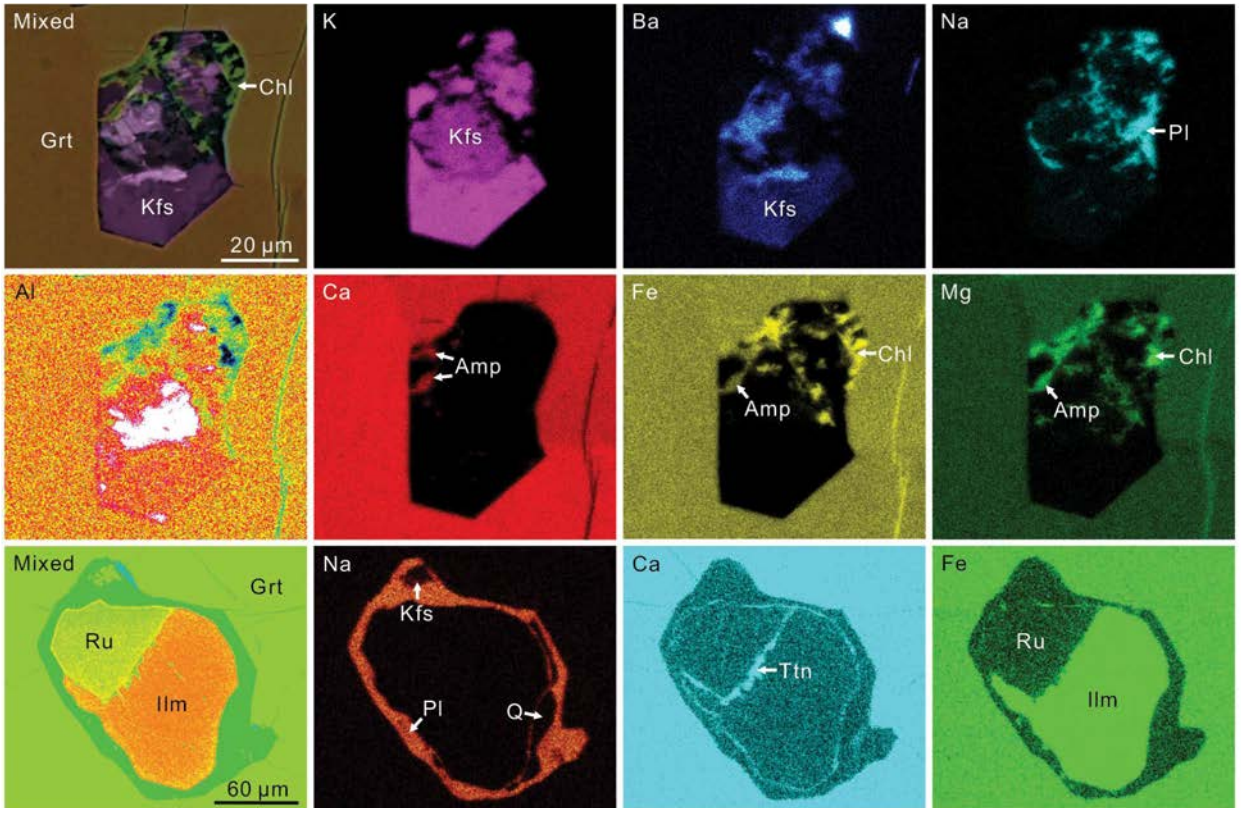

FIGURE 4. Mixed mapping images and single element mapping images of two PSIs (EDX mode). See their BSE images in Figures 3i and 3m, respectively. (Color online.)

responsible for the formation of the quartz-garnet veins, which include: (1) circulated fluids directly precipitating new minerals in the open fractures; (2) flux melting (i.e., a melting process that involves infiltration of external water and other volatile components into a solid rock) of the original eclogite within the fracture zones; and (3) leaching of the original eclogite by passing fluids along the fracture zones. Garnet in the veins contains the same mineral (e.g., coesite) inclusions as that in the eclogite (Figs. 1c, 2a, and 2b), and often displays a resorption texture along its rim. In addition, both garnets share virtually the same major and trace element chemistry (Supplemental[1] Tables S1 and S2; Figs. 6a and 7a). These features indicate that garnet in the veins is an original mineral from the eclogite instead of a newly precipitated mineral. Thus, process (1) is not supported by evidence. The texture of amphibole + plagioclase symplectites in the eclogite is not disturbed by the quartz-garnet veins at the eclogite-vein boundaries indicating that the veins were formed at an eclogite-facies stage before the amphibolite-facies overprint. Extensive occurrence of plagioclase in the quartz-garnet veins (Figs. 1e and 1f) further constrains the formation of the veins at lower pressures than those at the reaction curve of albite = jadeite + quartz. Corresponding to such a late metamorphic stage, the retrograde *P-T* paths constructed for the eclogite and surrounding marble could have overstepped the wet solidus of a common eclogite (Fig. 8). However, a high degree of melting is required to remove a significant quantity of the original omphacite (and dolomite) in the fracture zones to produce a garnet-rich vein. Thus, the relatively low temperature around 650 °C leaves a significant water influx (i.e., a high water/rock ratio) as the only choice to comprehend the formation of quartz-garnet veins in the eclogite. In such a case, a dissolution-dominated leaching process should have played a dominant role in forming these veins instead of partial melting. If the *P-T* path has never overstepped the wet solidus of a common eclogite, a dissolution-dominated leaching process can be the only candidate as formation mechanism for the veins.

According to the above considerations the quartz-garnet veins formed as follows: (1) Fractures were opened in the host eclogite during early exhumation. (2) External aqueous fluids were introduced under eclogite-facies conditions, leading to a local high water/rock ratio in and near the fracture zones. (3) Omphacite, dolomite ± other minerals in these zones were dissolved in the fluids that then precipitated new plagioclase and net quartz. (4) Garnet in the fractures zones survived the dissolution process and were enriched in the leached zones to finally form the quartz-garnet veins.

A NEW MODEL FOR THE FORMATION OF PSIS

PSIs in this study display wedge-like offshoot and protrusion textures and inclusion-garnet interfaces controlled by the crystallographic structure of garnet (Fig. 3). These microstructures are similar to those of primary PSIs found in UHP (e.g., Stöckhert et al. 2001, 2009; Ferrando et al. 2005; Korsakov and Hermann 2006; Frezzotti et al. 2007; Frezzotti and Ferrando 2015) and anatectic rocks (e.g., Cesare et al. 2009, 2015; Ferrero et al.

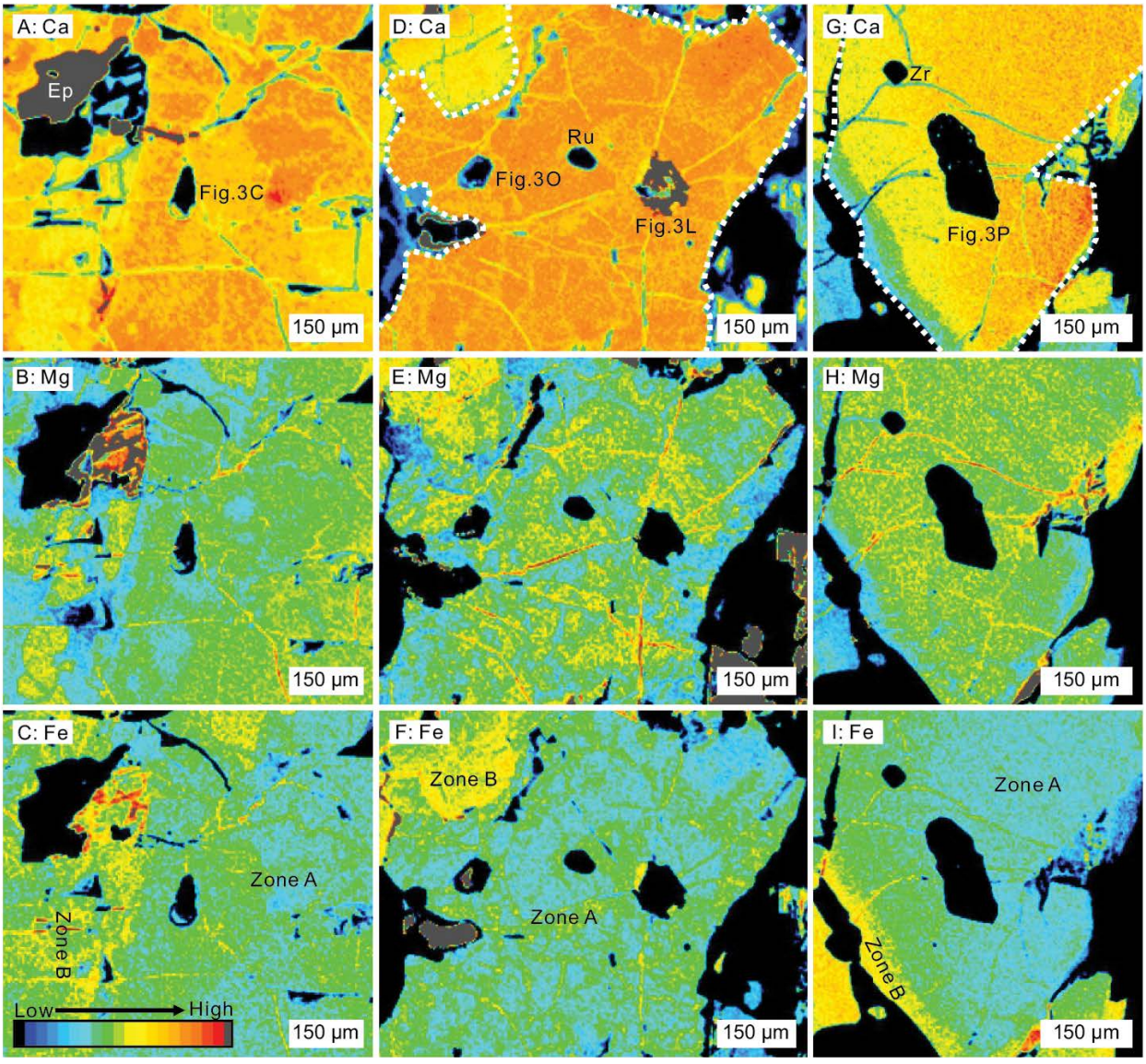

FIGURE 5. Element mapping images of three garnet grains containing PSIs (WDX mode). The garnet rim was altered by fluids with zones A and B representing the original and the altered domains, respectively. Note that PSIs only occur in zone A and did not cause any compositional alteration of garnet. In **d** and **g**, the two garnet grains containing PSIs are outlined, where in **a** only part of a single PSI-bearing garnet grain is shown. (Color online.)

2012, 2015; Bartoli et al. 2013), which could be best explained by fluid-mediated shape maturation and decrepitation of fluid-bearing inclusions within garnet (e.g., Roedder 1984; Perchuk et al. 2005; Ferrero et al. 2012). Nevertheless, the investigated PSIs differ from the previous primary ones in several aspects. Primary PSIs are formed by entrapment of a fluid phase in a growing garnet and, thus, usually share the following features: (1) occurrence of inclusions in clusters in a specific domain of garnet; (2) display of a constant polycrystalline mineral assemblage and (3) of a negative crystal shape (an isometric shape with rhombododecahedral geometry). To be compared, PSIs in this study are distributed randomly in garnet and a single garnet grain only contains one (Fig. 1f) to several of them. In addition, the kind of the constituting minerals and their proportions vary considerably in our PSIs (Fig. 3). Even though some inclusion-garnet interfaces reflect the crystallographic control of the host mineral, PSIs in this study show a typical negative crystal shape rarely (Fig. 3). Therefore, a formation mechanism different from that of the primary PSIs is indicated for the investigated PSIs.

Type-1 and Type-2 PSIs sometimes display a prismatic or a platy shape (Figs. 3a, 3c–3e, 3h, 3j, and 3r), which is compatible with that of euhedral coesite inclusions. This leads us to believe that external fluids could have infiltrated the host garnet along its fractures and reacted with the precursor coesite inclusions, thereby inheriting their shapes. Such an explanation is validated by the microstructures of Type-3 PSIs (Figs. 3m–3p and 3t).

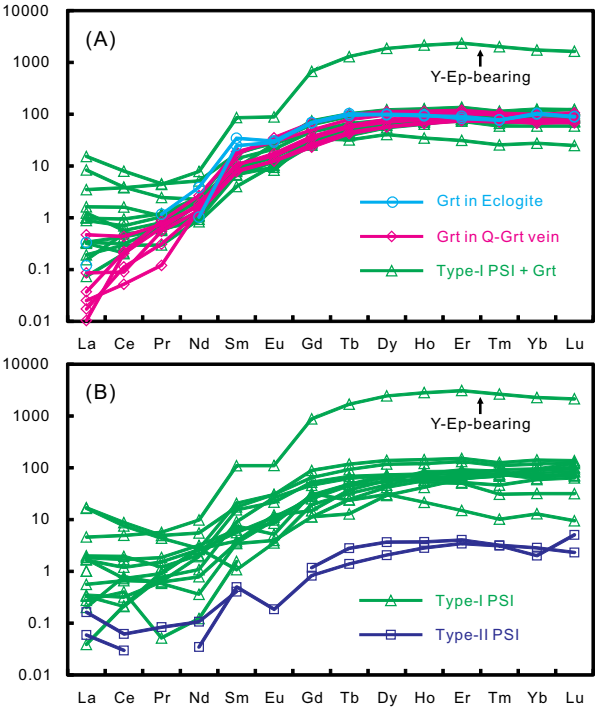

FIGURE 6. Chondrite-normalized REE patterns of garnet and PSIs: (**a**) unaltered garnet and mixtures of Type-1 PSI + unaltered garnet; (**b**) calculated Type-1 and Type-2 PSIs. Chondrite values are from Sun and McDonough (1989). (Color online.)

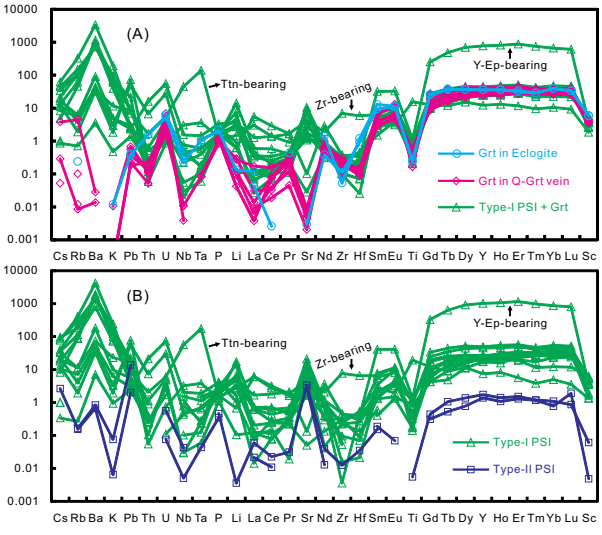

FIGURE 7. Primitive mantle-normalized spider diagrams of garnet and PSIs: (**a**) unaltered garnet and mixtures of Type-1 PSI + unaltered garnet; (**b**) calculated Type-1 and Type-2 PSIs. Primitive mantle values are from McDonough and Sun (1995). (Color online.)

The rutile (± ilmenite ± titanite) core within these PSIs is too large to be a daughter mineral precipitated from an entrapped fluid. The rutile core is surrounded by feldspars ± quartz and the whole inclusion always exhibits the general morphology of the rutile core. These features suggest that a single rutile grain

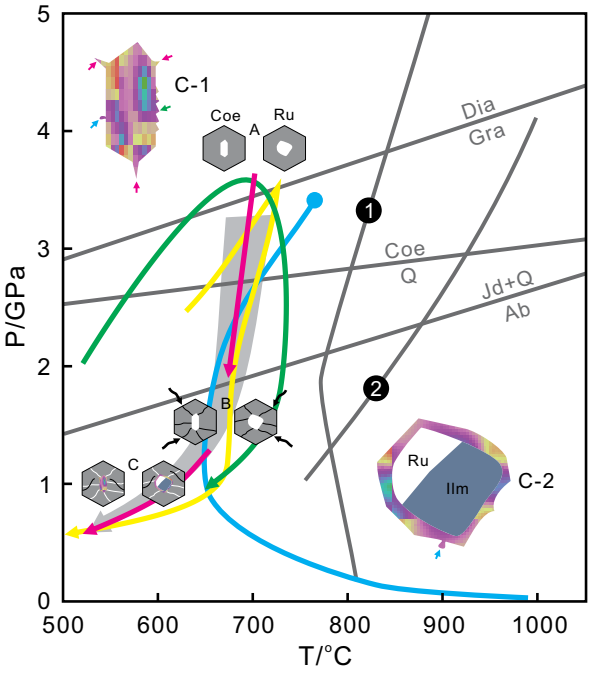

FIGURE 8. Petrogenesis of PSIs in this study. Coesite and rutile were enclosed by growing garnet during prograde metamorphism (before stage A). From stage A to B, early fractures opened in garnet along which the external fluids infiltrated the mineral inclusions. Then, interactions between fluid, inclusion, and garnet were initiated and continued until stage C. The early fractures (white lines) had been healed and two representative PSIs were produced. New fractures (black lines) opened later on. C-1 and C-2 are the two PSIs at stage C, which are enlarged to highlight their microstructures. Wedge-like offshoot and protrusion textures and serrate inclusion-garnet interfaces are indicated by pink, light blue, and green arrows, respectively. Phase-transition curves of diamond = graphite, coesite = quartz, and albite = jadeite + quartz are after Bundy (1980), Bohlen and Boettcher (1982), and Li et al. (2004), respectively. Curves 1 and 2 are the phengite-dehydration melting curves in metagreywacke (Auzanneau et al. 2006) and eclogite (Liu et al. 2009), respectively. Arrow lines are *P-T* paths constructed for the Dabie UHP eclogites: pink = this study, green = Carswell and Zhang (1999), gray = Zhang et al. (2003), and yellow = Rolfo et al. (2004). The blue line refers to the wet basalt solidus after Lambert and Wyllie (1972). The blue solid circle is the second critical point of basalt after Mibe et al. (2011). (Color online.)

was once enclosed in garnet and external fluids infiltrated this inclusion along the rutile-garnet interfaces. In response to this infiltration, material was dissolved from the host garnet and/or the rutile core to enlarge the space for accommodating the newly precipitated feldspars ± quartz. Whether this process was accompanied by the partial replacement of rutile by ilmenite and titanite must be called in question. As outlined above, the fluid infiltration occurred still at conditions of the eclogite-facies. At such conditions, rutile is the stable Ti-mineral, but local equilibria leading to the formation of ilmenite and/or titanite already in the eclogite-facies cannot be ruled out. Concerning PSIs without typical coesite morphologies or rutile cores, the former presence of other mineral inclusions (e.g., omphacite and phengite; see Fig. 8 in Gao et al. 2014) is possible. The extant fractures in garnet could have served as the infiltration pathways for the fluids into

the former mineral inclusions. If this was the case, some of these fractures should have been filled by minerals (such as feldspar) that are also present in the PSIs, not by chlorite that formed during very late alteration (Fig. 3q). Therefore, the possibility of fluids infiltrating along the extant fractures can be ruled out. BSE-brighter vein-like domains occur around the PSIs in garnet (Figs. 3e, 3f, 3k, and 3l), which are explained to represent early fractures that were healed during fluid-garnet interactions. In our opinion, these early fractures are to be considered as the pathways for the fluid infiltration.

A detailed model on the formation of the studied PSIs is shown in Figure 8. Coesite, rutile, and other metamorphic minerals were captured by growing garnet during prograde metamorphism (before stage A). During early decompression (from stage A to B), early fractures were created in garnet because of hydrofracturing and/or differential expansion of mineral inclusions relative to the host garnet (see Whitney 1996). At stage B when the quartz-garnet veins were formed, aqueous fluids infiltrated the mineral inclusions along the early fractures and interacted with them and the host garnet via a dissolution-reprecipitation mechanism. As a microstructural response, the inclusion-garnet interfaces were adjusted to reduce the surface free energy (Roedder 1984), resulting in straight, serrate, and smooth inclusion walls. Later decrepitation could lead to wedge-like offshoot and/or protrusion textures. The external fluid-mineral inclusion-host garnet interaction continued until the amphibolite-facies stage C was reached. The early fractures had been healed and our two representative PSIs were formed. It should be noted that some monophase quartz inclusions after coesite display microstructures reflecting a similar fluid-mediated process (Fig. 2). These quartz inclusions and Type-1 PSIs are interpreted to represent a continuous product series by interaction between the precursor coesite inclusions and the infiltrating fluids. Monophase quartz inclusions were instead formed when no new mineral was precipitated from this interaction.

Coupled to the variation of constituent minerals and their contents within the PSIs (Fig. 3), the bulk composition of the PSIs varies considerably even if we only consider Type-1 PSIs (Figs. 6 and 7). Such variations can be hardly interpreted as the result of a primary entrapment process but can be explained using our new model: (1) the former mineral (e.g., coesite, omphacite, phengite) inclusions changed from one case to the other; (2) infiltrating fluids reacted with the former mineral inclusions and host garnet to different degrees; and (3) the fluid composition evolved with the fluid-rock interaction. As discussed in the subsequent section, more than one type of fluid phase had been involved in the PSI formation, which could have also contributed to such variations.

Nature of fluids involved in the PSI formation

Recent studies proposed that Type-1 PSIs represent silicate melts derived from dehydration melting of phengite and/or paragonite (e.g., Zeng et al. 2009; Gao et al. 2012, 2013, 2017; Liu et al. 2013; Chen et al. 2014; Wang et al. 2016). In addition, calcite in Type-2 PSIs was considered to reflect partial melting of subducted carbonates (Gao et al. 2014). Nevertheless, no good arguments were given in these studies why these PSIs should represent melts instead of aqueous fluids except that a *P-T* path was envisaged to cross the dehydration melting curve of phengite. As seen in Figure 8, the newly constructed *P-T* path is just like earlier ones obtained for different UHP eclogites from the Dabie Shan (e.g., Carswell and Zhang 1999; Zhang et al. 2003; Rolfo et al. 2004). These paths do hardly cross the dehydration melting curve of phengite. Instead of flux melting, we propose that a dissolution-dominated leaching process played the key role in forming the PSI-bearing veins. This means that aqueous fluids instead of melts should have been formed and dominated the fluid phase in the veins. Compared with silicate melts, aqueous fluids have much lower viscosities (Audétat and Keppler 2004) and could more easily infiltrate the former mineral inclusions along garnet fractures. Silicate melts, if they were really present and have dominated the fluid phase responsible for the formation of PSIs, should have been felsic. Type-3 PSIs should have, thus, contained quartz as a common mineral that resulted from the melt crystallization (Type-1 and Type-2 PSIs cannot give an unambiguous indication in this situation). However, this is not the case (Figs. 3m–3p and 3t). Besides, dark and/or white mica are common crystallization products of felsic melt inclusions (e.g., Cesare et al. 2009, 2015; Ferrero et al. 2012, 2015; Bartoli et al. 2013), which are absent in the studied PSIs (Fig. 3; also see Zeng et al. 2009; Gao et al. 2012, 2013, 2017; Liu et al. 2013; Chen et al. 2014). K-feldspar within the studied PSIs contains up to 14.5 wt% BaO (Supplemental[1] Table S1). Such Ba-rich K-feldspar has been also documented for similar PSIs in other studies (e.g., Yang et al. 1998; Zeng et al. 2009; Gao et al. 2012; Liu et al. 2013; Chen et al. 2014; Wang et al. 2016). It is noteworthy that the occurrence of Ba-rich K-feldspar is often reported to be related to the activities of aqueous fluids (e.g., Harlov et al. 1998; Moro et al. 2001; Shi et al. 2010; Henry and Will 2015). This relation is compatible with the fact that Ba is highly compatible in aqueous fluids (e.g., Green and Adam 2003; Kessel et al. 2005; Tsay et al. 2017). Thus, Ba-rich K-feldspar within the studied PSIs provides another argument that fluids involved in the formation of these PSIs were aqueous fluids instead of hydrous melts.

Related to the fluid nature and the formation of Type-3 PSIs, the efficiency of material removal from the rutile inclusions and the host garnet (see above) must be considered. At given *P-T* conditions, the solubility of Ti in aqueous fluids largely depends on the fluid chemistry. For example, high F concentrations can significantly enhance the solubility of Ti in aqueous fluids (e.g., Rapp et al. 2010). However, the efficiency of Ti removal from the rutile inclusions by aqueous fluids depends not only on its solubility but also on time. As long as the disequilibrium state was maintained between the infiltrating fluids and the rutile inclusions while the garnet fractures stayed open, chemical gradients in the fluids could lead to the continuous removal of Ti from the rutile inclusions. This explanation can be applied to the partial removal of garnet as well. Dissolution of rutile and garnet did not produce any new Ti- or FeMg-bearing mineral in Type-3 PSIs probably because chemical gradients in the fluids could not result in saturation of these elements at the dissolving site, i.e., the dissolved elements of Ti-Fe-Mg would diffuse away from the dissolving site.

In the light of our new model described above, recovering the composition of the interacting aqueous fluids through analyzing the bulk composition of the PSIs is nearly impossible unless the bulk distribution coefficient of each element between such fluids

and the PSIs is known. Besides, we have to consider the possibility of disequilibrium between the newly precipitated minerals and the fluids. Nevertheless, we can still put some compositional constraints on the interacting aqueous fluids. Precipitation of feldspars in Type-1 and Type-3 PSIs indicate that the aqueous fluids were rich in Si-Al-Na-K components. Calcite in Type-2 PSIs suggests that a second immiscible aqueous fluid rich in carbon could have been present. Regarding trace elements, Figures 6 and 7 indicate that the siliceous aqueous fluids were rich in LILEs (Cs, Rb, Ba, K, Pb, Li, Sr) and that the carbonaceous fluids were rich in Pb and Sr. Such fluids were probably, at a first stage, generated in the subducting oceanic crust at great depths but relatively low temperatures and then infiltrated hotter rocks that were exhumed in a subduction channel (see Massonne 2012; Liu et al. 2017b) such as the eclogite investigated here.

IMPLICATIONS

In this study, a new model was proposed for the formation of polyphase solid-inclusions (PSIs) that allows us to trace the fluid evolution and post-entrapment modifications of mineral inclusions (such as coesite) in high-pressure and ultrahigh-pressure metamorphic rocks. This new model indicates that PSIs enclosed in peak minerals (particularly those showing fractures and/or healed fractures) of such rocks are not always primary as previously thought and that PSIs do not necessarily represent entrapped supercritical fluid or melt inclusions. In addition, we conclude that recovering the fluid composition through integrating the bulk composition of this kind of PSIs should be cautiously done (see Gao et al. 2012, 2013, 2014, 2017; Liu et al. 2013; Chen et al. 2014), although certain geochemical fingerprints can be qualitatively traced.

ACKNOWLEDGMENTS

We thank S. Zheng (Wuhan) and T. Theye (Stuttgart) for assistance with the EMP and T. Luo (Wuhan) for help with the LA-ICP-MS analyses. This study was funded by grant from the National Key Basic Research Program of China (No. 2015CB856101). Thorough reviews by S. Ferrero, I. Klonowska, and an anonymous reviewer as well as careful editorial handling by K. Ashley are gratefully acknowledged.

REFERENCES CITED

Audétat, A., and Keppler, H. (2004) Viscosity of fluids in subduction zones. Science, 303, 513–516.

Auzanneau, E., Vielzeuf, D., and Schmidt, M.W. (2006) Experimental evidence of decompression melting during exhumation of subducted continental crust. Contributions to Mineralogy and Petrology, 152, 125–148.

Bartoli, O., Cesare, B., Poli, S., Bodnar, R.J., Acosta-Vigil, A., Frezzotti, M.L., and Meli, S. (2013) Recovering the composition of melt and the fluid regime at the onset of crustal anatexis and S-type granite formation. Geology, 41, 115–118.

Bohlen, S.R., and Boettcher, A.L. (1982) The quartz-coesite transformation: a pressure determination and the effects of other components. Journal of Geophysical Research, 87, 7073–7078.

Bundy, F.P. (1980) The *P*, *T* phase and reaction diagram for elemental carbon. Journal of Geophysical Research, 85, 7073–7078.

Carswell, D.A., and Zhang, R.Y. (1999) Petrographic characteristics and metamorphic evolution of ultrahigh-pressure eclogites in plate-collision belts. International Geology Review, 41, 781–798.

Cesare, B., Ferrero, S., Salvioli-Mariani, E., Pedron, D., and Cavallo, A. (2009) "Nanogranite" and glassy inclusions: The anatectic melt in migmatites and granulites. Geology, 37, 627–630.

Cesare, B., Acosta-Vigil, A., Bartoli, O., and Ferrero, S. (2015) What can we learn from melt inclusions in migmatites and granulite? Lithos, 239, 186–216.

Chen, Y.X., Zheng, Y.F., Gao, X.Y., and Hu, Z.C. (2014) Multiphase solid inclusions in zoisite-bearing eclogite: evidence for partial melting of ultrahigh-pressure metamorphic rocks during continental collision. Lithos, 200-201, 1–21.

Ferrando, S., Frezzotti, M.L., Dallai, L., and Compagnoni, R. (2005) Multiphase solid inclusions in UHP rocks (Su-Lu, China): remnants of supercritical silicate-rich aqueous fluids released during continental subduction. Chemical Geology, 223, 68–81.

Ferrero, S., Bartoli, O., Cesare, B., Salvioli-Mariani, E., Acosta-Vigil, A., Cavallo, A., Groppo, C., and Battiston, S. (2012) Microstructures of melt inclusions in anatectic metasedimentary rocks. Journal of Metamorphic Geology, 30, 303–322.

Ferrero, S., Wunder, B., Walczak, K., O'Brien, R.J., and Ziemann, M.A. (2015) Preserved near ultrahigh-pressure melt from continental crust subducted to mantle depths. Geology, 43, 447–450.

Frezzotti, M.L., and Ferrando, S. (2015) The chemical behavior of fluids released during deep subduction based on fluid inclusions. American Mineralogist, 100, 352–377.

Frezzotti, M.L., Ferrando, S., Dallai, L., and Compagnoni, R. (2007) Intermediate alkali-alumino-silicate aqueous solutions released by deeply subducted continental crust: fluid evolution in UHP OH-rich topaz-kyanite quartzites from Donghai (Sulu, China). Journal of Petrology, 48, 1219–1241.

Gao, X.Y., Zheng, Y.F., and Chen, Y.X. (2012) Dehydration melting of ultrahigh-pressure eclogite in the Dabie orogen: evidence from multiphase solid inclusions in garnet. Journal of Metamorphic Geology, 30, 193–212.

Gao, X.Y., Zheng, Y.F., Chen, Y.X., and Hu, Z.C. (2013) Trace element composition of continentally subducted slab-derived melt: insight from multiphase solid inclusions in ultrahigh-pressure eclogite in the Dabie orogeny. Journal of Metamorphic Geology, 31, 453–468.

——— (2014) Composite carbonate and silicate multiphase solid inclusions in metamorphic garnet from ultrahigh-*P* eclogite in the Dabie orogen. Journal of Metamorphic Geology, 32, 961–980.

Gao, X.Y., Chen, Y.X., and Zhang, Q.Q. (2017) Multiphase solid inclusions in ultrahigh-pressure metamorphic rocks: A snapshot of anatectic melts during continental collision. Journal of Asian Earth Sciences, 145, 192–204.

Green, T.H., and Adam, J. (2003) Experimentally-determined trace element characteristics of aqueous fluid from dehydrated mafic oceanic crust at 3.0 GPa, 650-700 °C. European Journal of Mineralogy, 15, 815–830.

Harlov, D.E., Hansen, E.C., and Bigler, C. (1998) Petrologic evidence for K-feldspar metasomatism in granulite facies rocks. Chemical Geology, 151, 373–386.

Henry, D.J., and Will, C.N. (2015) Ba-rich K-feldspar from mafic xenoliths within Mesoarchean granitic rocks, Beartooth Mountains, Montana, USA: indicators for barium metasomatism. Canadian Mineralogist, 53, 185–198.

Hermann, J., and Rubatto, D. (2014) Subduction of continental crust to mantle depth: geochemistry of ultrahigh-pressure rocks. In HD. Holland and K.K. Turekian, Treatise on Geochemistry, 2nd ed., vol. 4, p. 309–340. Elsevier, Oxford.

Hermann, J., Zheng, Y.F., and Rubatto, D. (2013) Deep fluids in subducted continental crust. Elements, 9, 281–287.

Hwang, S.L., Shen, P.Y., Chu, H.T., Yui, T.F., and Lin, C.C. (2001) Genesis of microdiamonds from melt and associated multiphase inclusions in garnet of ultrahigh-pressure gneiss from Erzgebirge, Germany. Earth and Planetary Science Letters, 188, 9–15.

Kessel, R., Schmidt, M.W., Ulmer, P., and Pettke, T. (2005) Trace element signature of subduction-zone fluids, melts and supercritical liquids at 120–180 km depth. Nature, 437, 724–727.

Korsakov, A.V., and Hermann, J. (2006) Silicate and carbonate melt inclusions associated with diamonds in deeply subducted carbonate rocks. Earth and Planetary Science Letters, 241, 104–118.

Labrousse, L., Prouteau, G., and Ganzhorn, A.C. (2011) Continental exhumation triggered by partial melting at ultrahigh pressure. Geology, 39, 1171–1174.

Lambert, I.B., and Wyllie, P.J. (1972) Melting of gabbro (quartz eclogite) with excess water to 35 kilobars, with geological applications. Journal of Geology, 80, 693–708.

Leake, B.E., Woolley, A.R., Arps, C.E.S., Birch, W.D., Gilbert, M.C., Grice, J.D., Hawthorne, F.C., Kato, A., Kisch, H.J., Krivovichev, V.G., and others. (1997) Nomenclature of amphiboles: report of the subcommittee on amphiboles of the International Mineralogical Association Commission on New Minerals and Mineral Names. American Mineralogist, 61, 295–321.

Li, X.P., Zheng, Y.F., Wu, Y.B., Chen, F.K., Gong, B., and Li, Y.L. (2004) Low-*T* eclogite in the Dabie terrane of China: petrological and isotopic constraints on fluid activity and radiometric dating. Contributions to Mineralogy and Petrology, 148, 443–470.

Liu, Y.S., Hu, Z.C., Gao, S., Günther, D., Xu, J., Gao, C.G., and Chen, H.H. (2008) In situ analysis of major and trace elements of anhydrous minerals by LA-ICP-MS without applying an internal standard. Chemical Geology, 257, 34–43.

Liu, Q., Jin, Z.M., and Zhang, J.F. (2009) An experimental study of dehydration partial melting of a phengite-bearing eclogite at 1.5–3.0 GPa. Chinese Science Bulletin, 54, 2090–2100.

Liu, Q., Hermann, J., and Zhang, J. (2013) Polyphase inclusions in the Shuanghe UHP eclogites formed by subsolidus transformation and incipient melting during exhumation of deeply subducted crust. Lithos, 177, 91–109.

Liu, P.L., Wu, Y., Chen, Y., Zhang, J.F., and Jin, Z.M. (2015) UHP impure marbles from the Dabie Mountains: metamorphic evolution and carbon cycling in

continental subduction zones. Lithos, 212-215, 280–297.
Liu, P.L., Massonne, H.-J., Zhang, J.F., Wu, Y., and Jin, Z.M. (2017a) Intergranular coesite and coesite inclusions in dolomite from the Dabie Shan: constraints on the preservation of coesite in UHP rocks. Terra Nova, 29, 154–161.
Liu, P.L., Massonne, H.-J., Wu, Y., Jin, Z.M., and Zhang, J.F. (2017b) Diopside, apatite, and rutile in an ultrahigh pressure impure marble from the Dabie Shan, eastern China: A record of eclogite-facies metasomatism during exhumation. Chemical Geology, 466, 123–139.
Malaspina, N., Hermann, J., Scambelluri, M., and Compagnoni, R. (2006) Polyphase inclusions in garnet-orthopyroxenite (Dabie Shan, China) as monitors for metasomatism and fluid-related trace element transfer in subduction zone peridotite. Earth and Planetary Science Letters, 249, 173–187.
Massonne, H.-J. (2001) First find of coesite in the ultrahigh-pressure metamorphic area of the central Erzgebirge, Germany. European Journal of Mineralogy, 13, 565–570.
——— (2009) Hydration, dehydration, and melting of metamorphosed granitic and dioritic rocks at high- and ultrahigh-pressure conditions. Earth and Planetary Science Letters, 288, 244–254.
——— (2012) Formation of amphibole and clinozoisite-epidote in eclogite owing to fluid infiltration during exhumation in a subduction channel. Journal of Petrology, 53, 1969–1998.
Massonne, H.-J., and Nasdala, L. (2003) Characterization of an early metamorphic stage through inclusions in zircon of a diamondiferous quartzofeldspathic rock from the Erzgebirge, Germany. American Mineralogist, 88, 883–889.
McDonough, W.F., and Sun, S.S. (1995) The composition of the Earth. Chemical Geology, 120, 223–253.
Mibe, K., Kawamoto, T., Matsukage, K.N., Fei, Y.W., and Ono, S. (2011) Slab melting versus slab dehydration in subduction-zone magmatism. Proceedings of the National Academy of Sciences, 108, 8177–8182.
Moro, M.C., Cembranos, M.L., and Fernandez, A. (2001) Celsian, (Ba, K)-feldspar and cymrite from sedex barite deposits of Zamora, Spain. Canadian Mineralogist, 39, 1039–1051.
Perchuk, A.L., Burchard, M., Maresch, W.V., and Schertl, H.P. (2005) Fluid-mediated modification of garnet interiors under ultrahigh-pressure conditions. Terra Nova, 17, 545–553.
Proyer, A. (2003) The preservation of high-pressure rocks during exhumation: metagranites and metapelites. Lithos, 70, 183–194.
Rapp, J.F., Klemme, S., Butler, I.B., and Harley, S.L. (2010) Extremely high solubility of rutile in chloride and fluoride-bearing metamorphic fluids: An experimental investigation. Geology, 38, 323–326.
Roedder, E. (1984) Fluid Inclusions, Reviews in Mineralogy, 12, 678.
Rolfo, F., Compagnoni, R., Wu, W.P., and Xu, S.T. (2004) A coherent lithostratigraphic unit in the coesite-eclogite complex of Dabie Shan, China: geologic and petrologic evidence. Lithos, 73, 71–94.
Shi, G.H., Jiang, N., Wang, Y.W., Zhao, X., Wang, X., Li, G.W., Ng, E., and Cui, W.Y. (2010) Ba minerals in clinopyroxene rocks from the Myanmar jadeitite area: implications for Ba recycling in subduction zones. European Journal of Mineralogy, 22, 199–214.
Song, S.G., Yang, J.S., Xu, Z.Q., Liou, J.G., and Shi, R.D. (2003) Metamorphic evolution of the coesite-bearing ultrahigh-pressure terrane in the North Qaidam, Northern Tibet, NW China. Journal of Metamorphic Geology, 21, 631–644.
Stöckhert, B., Duyster, J., Trepmann, C., and Massonne, H.-J. (2001) Microdiamond daughter crystals precipitated from supercritical COH + silicate fluids included in garnet, Erzgebirge, Germany. Geology, 29, 391–394.
Stöckhert, B., Trepmann, C., and Massonne, H.-J. (2009) Decrepitated UHP fluid inclusions: about diverse phase assemblages and extreme decompression rates (Erzgebirge, Germany). Journal of Metamorphic Geology, 27, 673–684.
Sun, S.S., and McDonough, W.F. (1989) Chemical and isotopic systematics of oceanic basalts: implications for mantle composition and processes. Geological Society Special Publication, 42, 313–345.
Tsay, A., Zajacz, Z., Ulmer, P., and Sanchez-Valle, C. (2017) Mobility of major and trace elements in the eclogite-fluid system and element fluxes upon slab dehydration. Geochimica et Cosmochimica Acta, 198, 70–91.
Wang, S.J., Wang, L., Brown, M., and Feng, P. (2016) Multi-stage barite crystallization in partially melted UHP eclogite from the Sulu belt, China. American Mineralogist, 101, 564–579.
Whitney, D.L. (1996) Garnets as open systems during regional metamorphism. Geology, 24, 147–150.
Yang, J.J., Godard, G., and Smith, D.C. (1998) K-feldspar-bearing coesite pseudomorphs in an eclogite from Lanshantou (Eastern China). European Journal of Mineralogy, 10, 969–985.
Zeng, L.S., Liang, F.H., Asimow, P., Chen, F.Y., and Chen, J. (2009) Partial melting of deeply subducted continental crust and the formation of quartzofeldspathic polyphase inclusions in the Sulu UHP eclogites. Chinese Science Bulletin, 54, 2580–2594.
Zhang, J.F., Green, H.W., Bozhilov, K., and Jin, Z.M. (2004) Faulting induced by precipitation of water at grain boundaries in hot subducting oceanic crust. Nature, 428, 633–636.
Zhang, R.Y., Liou, J.G., Zheng, Y.F., and Fu, B. (2003) Transition of UHP eclogites to gneissic rocks of low-amphibolite facies during exhumation: evidence from the Dabie terrrane, central China. Lithos, 70, 269–291.
Zhang, R.Y., Liou, J.G., Iizuka, Y., and Yang, J.S. (2009) First record of K-cymrite in North Qaidam UHP eclogite, Western China. American Mineralogist, 94, 222–228.
Zheng, Y.F., Xia, Q.X., Chen, R.X., and Gao, X.Y. (2011) Partial melting, fluid supercriticality and element mobility in ultrahigh-pressure metamorphic rocks during continental collision. Earth-Science Reviews, 107, 342–374.

Manuscript received November 20, 2017
Manuscript accepted June 11, 2018
Manuscript handled by Kyle Ashley

Endnote:

[1]Deposit item AM-18-106395, Supplemental Tables. Deposit items are free to all readers and found on the MSA web site, via the specific issue's Table of Contents (go to http://www.minsocam.org/MSA/AmMin/TOC/2018/Oct2018_data/Oct2018_data.html).